frontiers | Frontiers in Earth Science

TYPE Original Research
PUBLISHED 22 March 2023
DOI 10.3389/feart.2023.1133413

OPEN ACCESS

EDITED BY
Shuai Yin,
Xi'an Shiyou University, China

REVIEWED BY
Kun Zhang,
Southwest Petroleum University, China
Qrong Qin,
Southwest Petroleum University, China

*CORRESPONDENCE
Lin Qi,
ejiqimao@163.com

SPECIALTY SECTION
This article was submitted to Structural Geology and Tectonics, a section of the journal Frontiers in Earth Science

RECEIVED 28 December 2022
ACCEPTED 20 February 2023
PUBLISHED 22 March 2023

CITATION
Lai Q, Qi L, Chen S, Ma S, Zhou Y, Fang P, Yu R, Li S, Huang J and Zheng J (2023), Resercoir space characteristics and pore structure of Jurassic Lianggaoshan Formation lacustrine shale reservoir in Sichuan Basin, China: Insights into controlling factors.
Front. Earth Sci. 11:1133413.
doi: 10.3389/feart.2023.1133413

Resercoir space characteristics and pore structure of Jurassic Lianggaoshan Formation lacustrine shale reservoir in Sichuan Basin, China: Insights into controlling factors

Qiang Lai[1], Lin Qi[1]*, Shi Chen[1], Shaoguang Ma[2], Yuanzhi Zhou[3], Pingchao Fang[3], Rui Yu[1], Shuang Li[4], Jun Huang[5] and Jie Zheng[6]

[1]Geology Exploration and Development Research Institute, CNPC Chuanqing Drilling Engineering Co., Ltd, Chengdu, China, [2]Development Department, PetroChina Southwest Oil and Gas Field Company, Chengdu, China, [3]Exploration Division, PetroChina Southwest Oil and Gas Field Company, Chengdu, China, [4]Sichuan Yuesheng Energy Group Co., Ltd, Chengdu, China, [5]Chengdu Geoservice Oil and Gas Technology Development Company, Chengdu, China, [6]Chengdu Caledonian Oil and Gas Technology Development Co., Ltd, Chengdu, China

The Jurassic Lianggaoshan Formation lacustrine shale oil is the most potential exploration target of unconventional hydrocarbon resource in Southwest China. In this study, nuclear magnetic resonance (NMR), scanning electron microscopy (SEM), low-temperature N_2 adsorption (LTNA), and high pressure mercury intrusion mercury injection capillary pressure are intergrated to reveal pore structure and its controlling factors of Lianggaoshan Formation lacustrine shale reservoir. Results indicate that three types of lithology combination are classified in the Jurassic Liangggaoshan lacustrine shale reservoir. Type A comprises pure shale. Type B is characterized by frequent shell limestone interbedding. Type C is characterized by frequent siltstone interbedding. The Type C shale is characterized by relatively high proportion of organic pores, high development and good connectivity of nanopores, and highest pore volume and Surface area. The nanopores of Lianggaoshan lacustrine shales are mainly dominated by mesopores and part of the macropores. Among them, the PV and SA are both mainly dominated by micropores. The enrichment of organic matter has little effect on the development of micropores, and does not affect the mesopore and macropore development. Quartz particles in Lianggaoshan lacustrine shale do not clearly facilitate the development of micropore and mesopore-macropore. Intraparticle pore in feldspar clast is an important component of mesopore and macropore. Clay minerals has no positive effect on the formation of micropore and mesopore-macropore.

KEYWORDS

fractal dimension, lacustrine shale, pore structure, lithology combination, lianggaoshan formation, Sichuan Basin

Introduction

Organic matter can be enriched in fine sediments in marine, transitional and lacustrine environments to form oil-bearing and natural gas-bearing organic shale (Gu et al., 2022a; Gu et al., 2022b; Gu et al., 2022c; Dong et al., 2022; Sun et al., 2022). At present, marine shale gas has achieved large-scale and efficient development (Zou et al., 2019; Li et al., 2022; Li et al., 2022; Li, 2022; Yuan et al., 2022). Fuling, Changning, Weiyuan, Zhaotong and other 100 billion square gas fields have been found in Sichuan Basin (Jiang et al., 2016; Jiang et al., 2018; Dong et al., 2022), forming the first 10 trillion square natural gas area in the history of China's petroleum industry in southern Sichuan (Fan et al., 2020; Fu et al., 2021; Fan et al., 2022). The exploration and development of lacustrine shale oil in China started relatively late, but due to the deepening of basic geological theory and the progress of engineering technology (Fu et al., 2020), significant exploration progress has been made in many sets of shale strata, such as the Paleogene Kongdian Formation and Shahejie Formation in the Bohai Bay Basin, the Permian Lucaogou Formation in Jimusar Sag, the Cretaceous Qingshankou shale of Songliao Basin, the Jurassic Dongyuemiao Member in Eastern Sichuan Basin, and the Triassic Yanchang shale in Ordos Basin (Yang et al., 2019; Wei et al., 2021; Peng et al., 2022; Qiu and He, 2022). Lacustrine shale oil in several basins has entered the stage of industrial development (Xu et al., 2017; Chen et al., 2018; Han et al., 2021; Zhao et al., 2022).

Due to the relatively small proportion of organic pores, lacustrine shale has more complex pore structure and stronger heterogeneity than marine shale (Zhang et al., 2021; Zhang et al., 2023). Intraparticle pores in clay aggregates, interparticle pores between or at the edges of brittle minerals (quartz or feldspar), and dissolution pores in calcite and dolomite are thought to provide the main storage space required for lacustrine shale oil (Zhang et al., 2020). The shale oil resources in the Sichuan Basin exceed two billion tons, and the shale quality is similar to that of other basins (Xu et al., 2017; Liu et al., 2021; Shu et al., 2021). Suggesting good exploration and development prospects (Wang et al., 2020). To date, the petroleum geologists have launched a new round of exploration work for the Lianggaoshan Formation shale oil. However, the study of lacustrine shale oil in the Sichuan Basin has just started, and the understanding is not deep (Xu et al., 2017; Liu et al., 2020). The Lianggaoshan Formation lacustrine shale experiences complex sedimentation and structural evolution, forming a large number of multiscale pore and fracture systems, so the heterogeneity of the reservoir pore structure is strong. Based on scanning electron microscopy (SEM), nuclear magnetic resonance (NMR), and related geochemical experiments, combined with low-temperature N_2 adsorption (LTNA) and mercury injection capillary pressure (MICP) measurement, this study quantitatively characterized the reservoir space and pore structure of the Lianggaoshan lacustrine shale in the Sichuan Basin by using the commonly used FHH model and analyzed the main influencing factors of the fractal dimension.

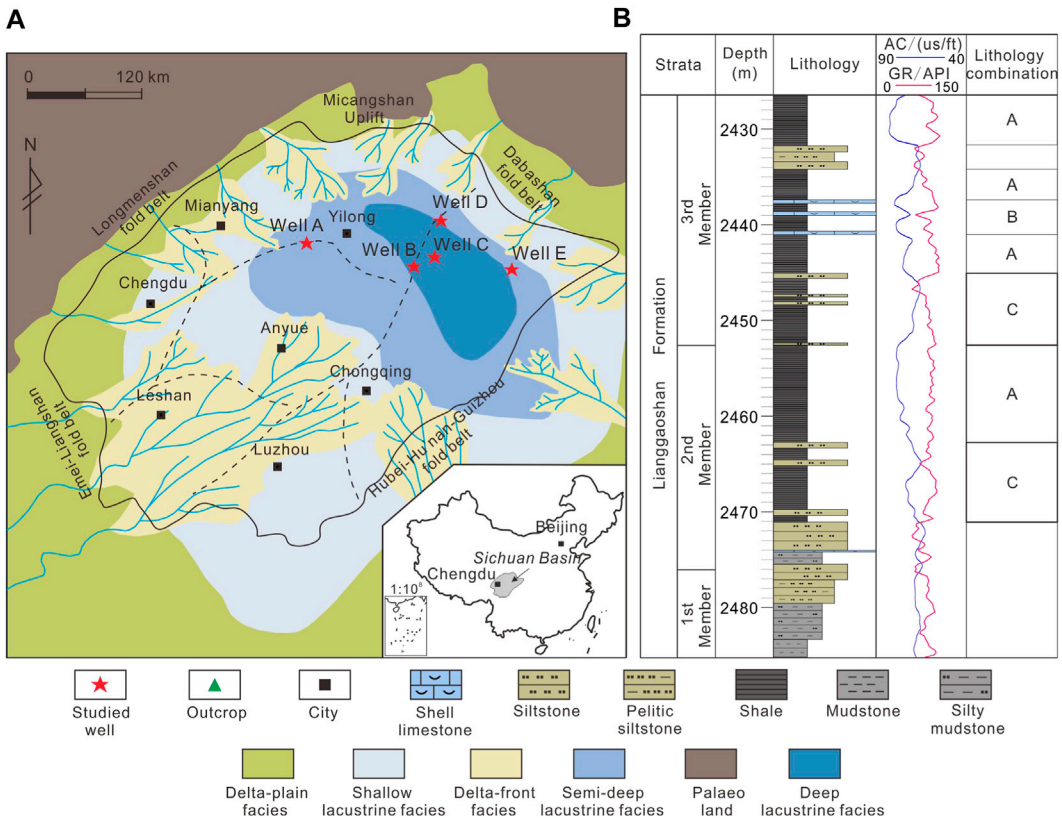

FIGURE 1
(A) Sedimentary facies of the Sichuan Basin during Lianggaoshan Formation deposition, Southwest China. **(B)** Generalized stratigraphy of Jurassic Lianggaoshan Formation Sichuan Basin (based on the Well B).

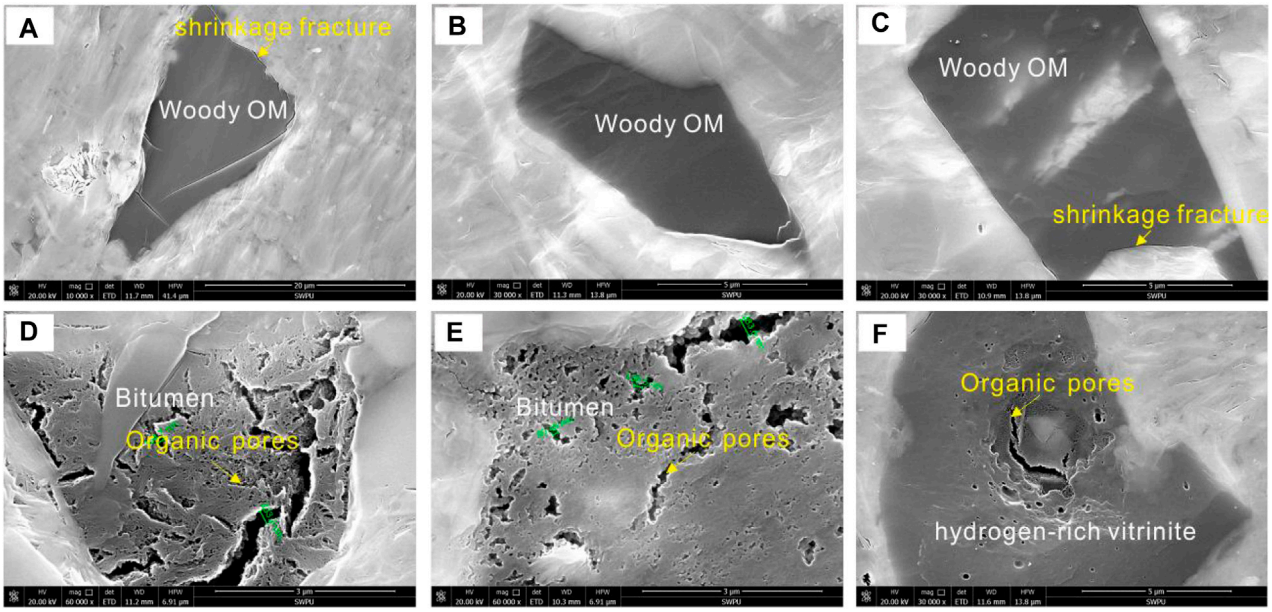

FIGURE 2
High-resolution SEM image of organic matters in Lianggaoshan Formation lacustrine shale reservoir. **(A)** No organic pores are developed in woody organic matter (OM), Type A shale, Well C, 2455.06m; **(B)** No organic pores are developed in woody organic matter (OM), Type A shale,Well B, 1896.13 m; **(C)** Only shrinkage fracture are oberved at the edge of woody organic matter (OM), Type B shale, Well C, 2452.29m; **(D)** Organic pores in bitumen, Type B shale, Well A, 1751.71 m; **(E)** Organic pores in bitumen, Type C shale, Well C, 2465.48m; **(F)** Organic pores in hydrogen-rich vitrinite, Type C shale, Well B, 1928.58 m

This study has guiding significance for geological evaluation of lacustrine shale reservoir.

Geological background

Sichuan Basin is located in the Southwest China (Figure 1A), and the area is about 260,000 km^2 (Figure 1A). In the Early-Middle Jurassic, the Sichuan Basin were dominated by a delta-lake sedimentary system and experienced four lake transgressions during this period (Cheng et al., 2023; Lei et al., 2023). From the bottom to the top, four sets of organic-rich shales formed in the Zhenzhuchong Member, Dongyuemiao Member, Da'anzhai Member, and Lianggaoshan Formation. The Lianggaoshan Formation comprises three members: first Member, second Member, and third Member. Within the range of lake deposition, the first Member and lower part of second Member are dominated by shore-shallow lake, and the third Member and upper part of second Member are dominated by semi-deep lake facies. Organic-rich shale is mainly developed in the upper part of second Member and third Member. According to the combination of rock types, the organic-rich shale can be divided into three types: Type A, Type B and Type C. Type A comprises pure shale, with clay content ranging between 20.4% and 65.4%. Type B is characterized by frequent shell limestone interbedding, with clay content ranging between 7.2% and 49.8%. Type C is characterized by frequent siltstone interbedding, with clay content ranging between 26.1% and 40.9% (Figure 1B).

Samples and methods

A total of 135 samples of Lianggaoshan lacustrine shale were acquired from drilling cores for SEM analysis, X-ray diffraction and TOC test. All experiments and measurements are finished in the PetroChina Exploration and Development Research Institute. The whole-rock and clay mineral X-ray diffraction measurement was carried out using a Malvern Panalytical X'Pert^3 MRD X-ray diffractometer. TOC test was finished through a LECO CS230 Series Carbon and Sulfur Analyzer. Mercury intrusion was finished through a Quantachrome Poremaster. Samples were prepared with an approximate size of 20 × 20 mm^2 and weighed out to 10–20 g, and then, the samples were dried at 110°C for at least 24 h under vacuum in an oven. The MICP ranged from 0 Mpa to 215 Mpa during this measurement. For low-temperature N_2 adsorption, the samples were crushed into 60–80 mesh, dried in an oven at 110°C for 12 h, and then placed in an Autosorb-IQ3 specific surface and a pore size distribution analyzer (Cantor Company, United States). The pretreatment was completed by degassing at 110°C for 12 h in the vacuum condition, and then nitrogen carbon adsorption was carried out. After the experiment, the Brunauer–Emmett–Teller (BET) model was used to calculate the specific surface area, and the Barrett–Joyner–Halenda (BJH) model was employed to obtain the pore size distribution and volume. The reservoir space classification is based on schemes proposed by Loucks et al. (2012). The pore size was divided into three categories according to the pore size distribution (Rouquerol et al., 1994): micropores (pore size < 2 nm), mesopores (pore size between 2nm and 50 nm), and macropores (pore size >50 nm).

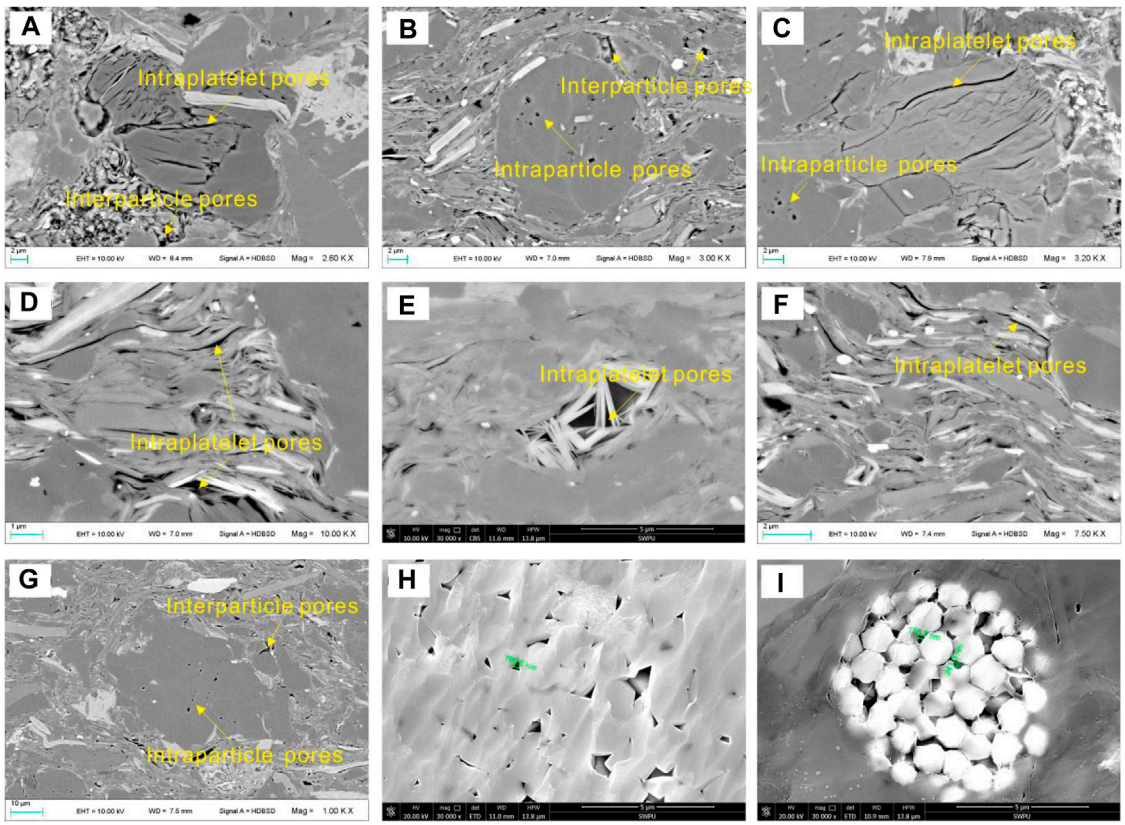

FIGURE 3
High-resolution SEM image of inorganic pores in Lianggaoshan Formation lacustrine shale reservoir. **(A)** Intraparticle pores in clay mineral aggregates, Type A shale, Well A, 2161.25m; **(B)** Intraparticle dissolution pores in feldspar granules, Type A shale, Well B, 2455.06m; **(C)** Type A shale, Well C, 1764.7m; **(D)** Intraparticle pores in clay mineral aggregates, Type B shale, Well D,2437.33 m; **(E)** Type B shale, Well B, 2452.29 m; **(F)** Type B shale, Well E, 1751.71 m; **(G)** Type C shale, Well A, 2164.49 m; **(H)** Type C shale, Well C, 1928.58 m; **(I)** Intercrystalline pores in strawberry pyrite aggregates, Type C shale, Well D, 2465.48 m

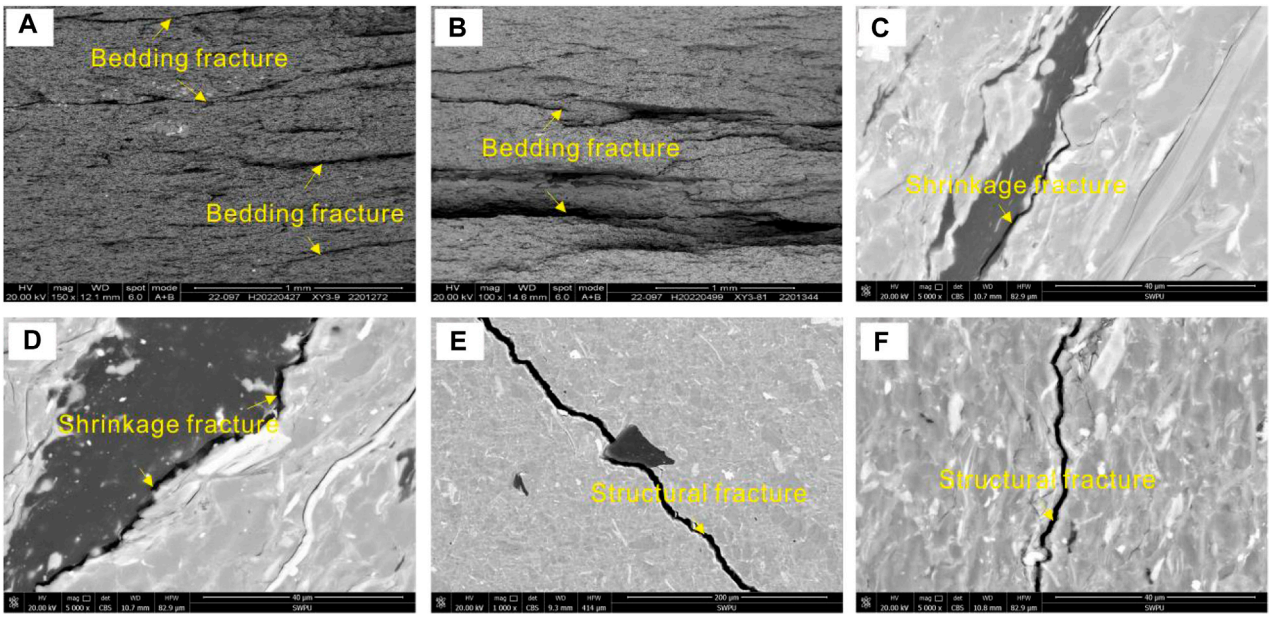

FIGURE 4
High-resolution SEM image of microfractures in Lianggaoshan Formation lacustrine shale reservoir. **(A)** Multiple bedding fracture are parallel to each other, Type A shale,Well C, 2455.06 m; **(B)** Bedding fracture in Type A shale,Well B, 1896.13 m; **(C)** Shrinkage fracture between organic matter and clay mineral, Type B shale,Well C, 2452.29 m; **(D)** Shrinkage fracture between organic matter and clay mineral, Type B shale,Well A, 1751.71 m; **(E)** Structural fracture in Type C shale, Well C, 2465.48 m; **(F)** Structural fracture in Type C shale, Well B, 1928.58 m.

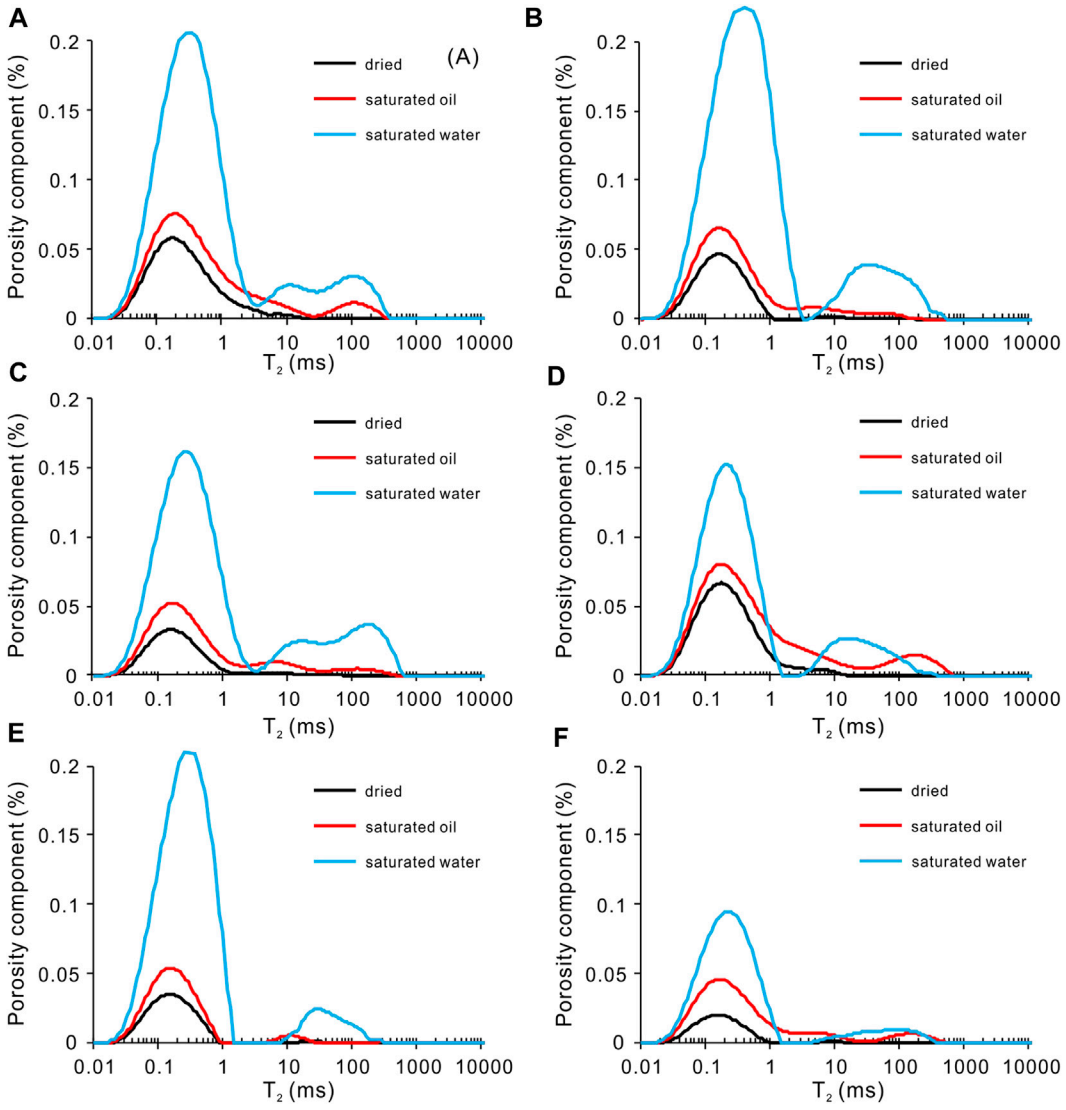

FIGURE 5
NMR T_2 spectra of Jurassic Lianggaoshan Formation lacustrine shale in different lithology combination under different states. **(A)** Type A shale,Well C, 2455.06m; **(B)** Type A shale,Well B, 1896.13 m; **(C)** Type B shale,Well C, 2452.29 m; **(D)** Type B shale,Well A, 1751.71 m; **(E)** Type C shale, Well C, 2465.48 m; **(F)** Type C shale, Well B, 1928.58 m.

When P/Po = 0.5, hysteresis loops of most samples begin to be observed, suggesting the great variation in pore size distribution (or morphology) causing different adsorption behaviors at this pressure (Guo et al., 2022a; Guo et al., 2022b; Li et al., 2022; Huang et al., 2022). The relative pressure (P/Po) was set as the threshold to divided the pore size distribution into two groups. The first group with P/Po=0-0.5 is subjected to the monolayer-multilayer adsorption process controlled by van der Waals force, while the second group with P/Po=0.5-1.0 experiences the capillary condensation adsorption process controlled by surface tension (Sun et al., 2015; Wang et al., 2015). In this paper, the Frenkel-Halsey-Hill (FHH) model is used to calculate the fractal dimensions of these two groups of samples separately, which are denoted as D_2 and D_1 for the first and second groups, respectively.

Results

Reservoir space characteristics

Organic pore

Organic pores are generally considered to be the main pore type of shale reservoirs and one of the key factors for shale gas enrichment (Xi et al., 2018; Cai et al., 2022; Wang et al., 2022; Xi et al., 2022). Organic matters in Lianggaoshan shale is mainly woody organic matter, followed by solid bitumen. The results of argon ion polishing scanning electron microscope show that the development of organic pores is different with different micro components. There are no organic pores in the woody organic matter (Figures 2A, B), but only shrinkage fracture at the edge of woody organic matter (Figure 2C). Both hydrogen-rich vitrinite and solid bitumen contain

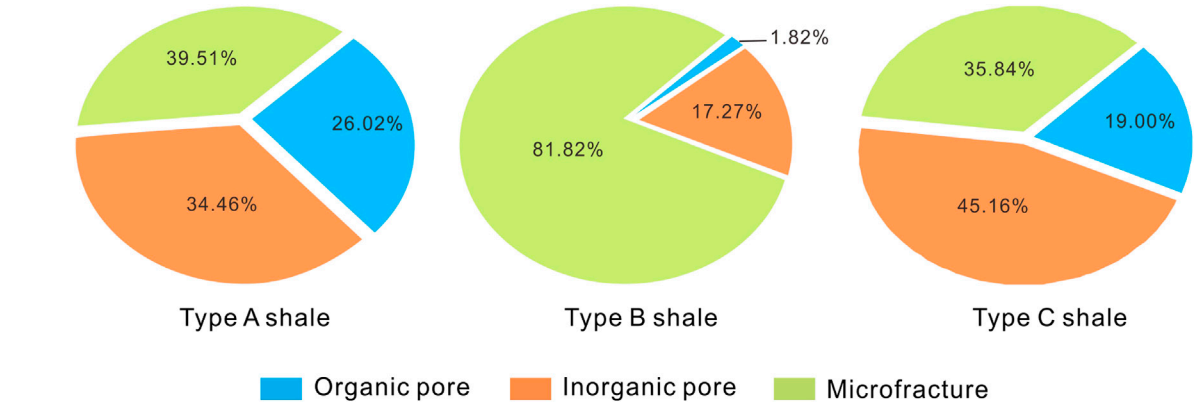

FIGURE 6
Histogram showing proportion of reservoir spaces of Jurassic Lianggaoshan Formation lacustrine shale in different lithology combination.

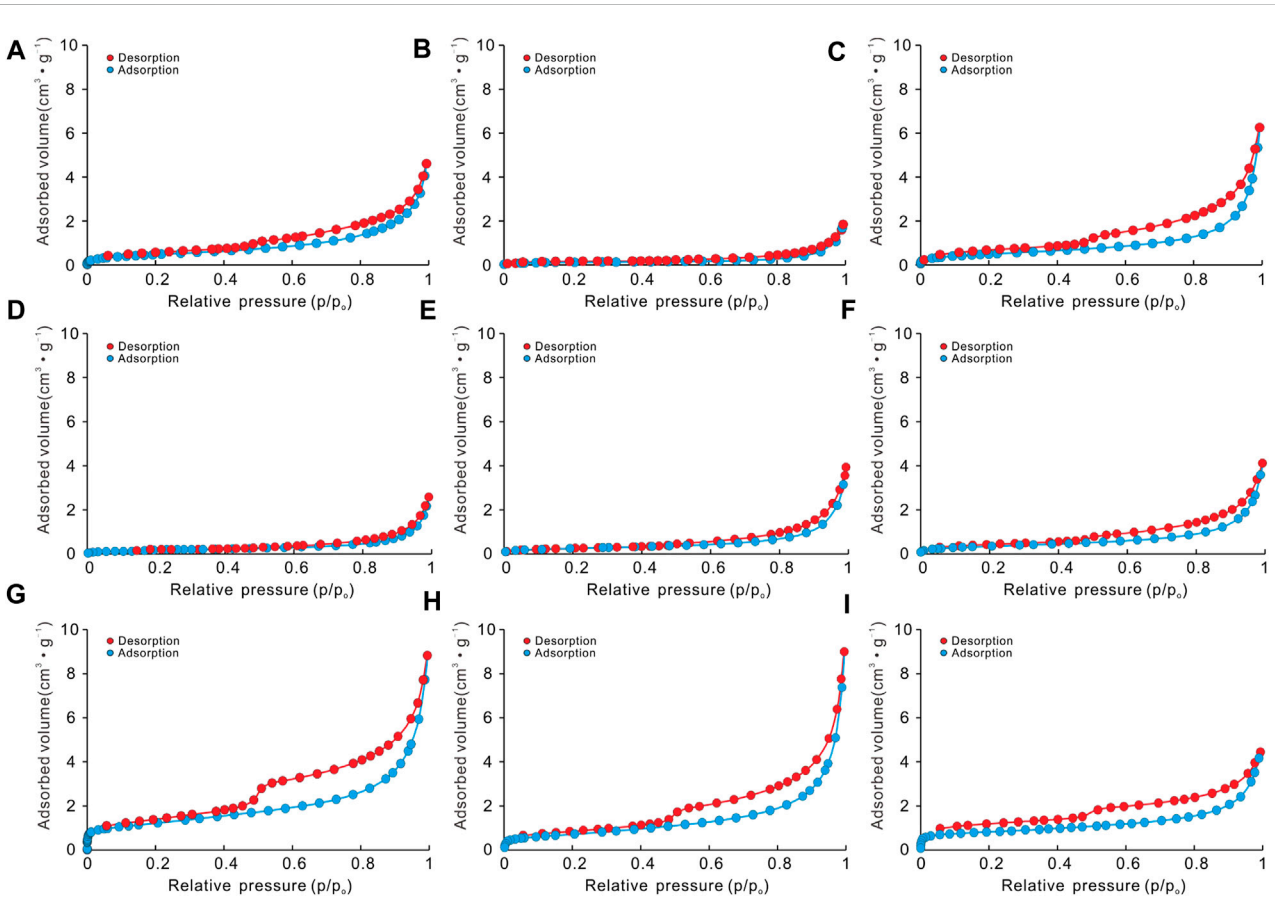

FIGURE 7
LTNA isotherms curves for the Lianggaoshan Formation lacustrine shale reservoir. **(A)** Type A shale, Well A, 2161.25 m; **(B)** Type A shale, Well B, 2455.06 m; **(C)** Type A shale, Well C, 1764.7 m; **(D)** Type B shale, Well D,2437.33 m; **(E)** Type B shale, Well B, 2452.29 m; **(F)** Type B shale, Well E, 1751.71 m; **(G)** Type C shale, Well A, 2164.49 m; **(H)** Type C shale, Well C, 1928.58 m; **(I)** Type C shale, Well D, 2465.48 m

varying degrees of round organic pores (Figures 2D, F). The development degree of shale organic pores in Type A and Type C shale is slightly higher (Figures 2D, E), mostly irregular, and the pore size is mostly 100nm–500 nm (Figure 2D). Type A shale locally develops honeycomb organic pores (Figure 2E), and the Type B shale organic pores are less developed (Figure 2F).

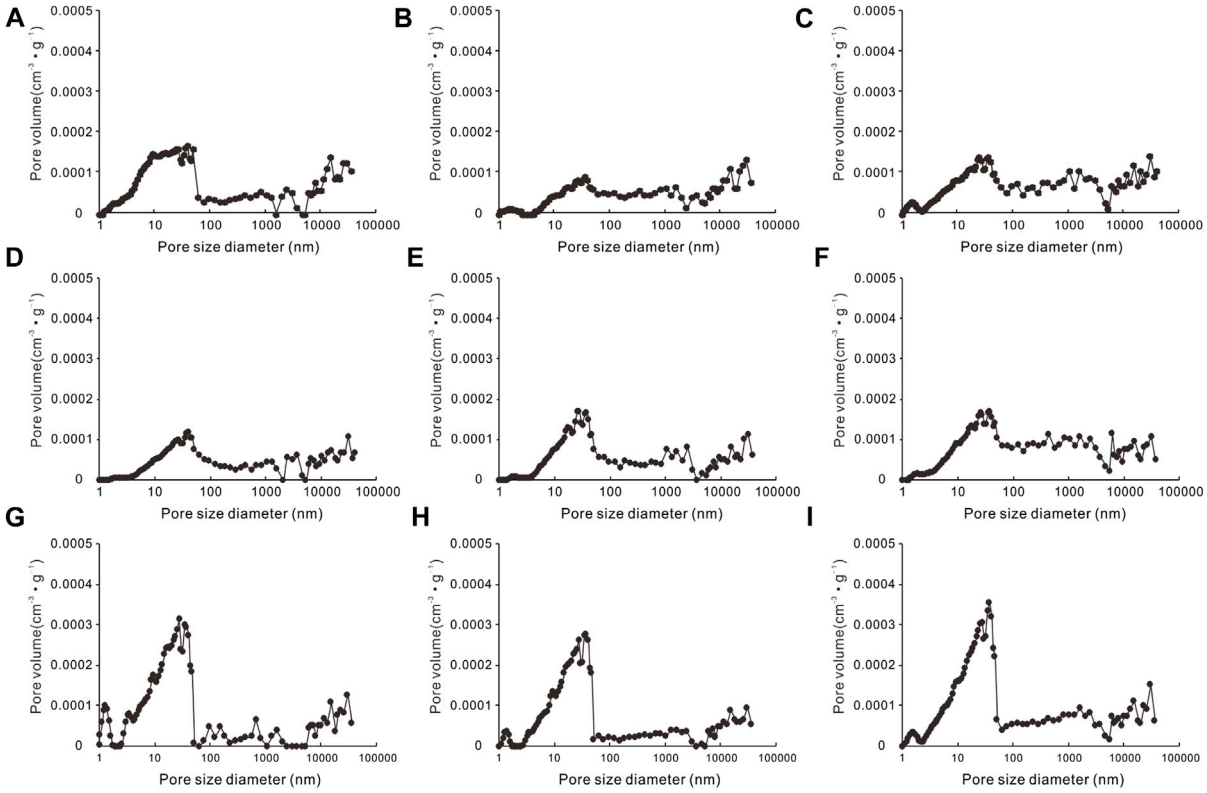

FIGURE 8
Pore-size distribution with MICP and LTNA for Jurassic Lianggaoshan Formation lacustrine shale in different lithology combination. **(A)** Type A shale, Well A, 2161.25 m; **(B)** Type A shale, Well B, 2455.06 m; **(C)** Type A shale, Well C,1896.18 m; **(D)** Type B shale, Well D, 2437.33 m; **(E)** Type B shale, Well B, 2452.29 m; **(F)** Type B shale, Well E, 1751.71 m; **(G)** Type C shale, Well A, 2164.49 m; **(H)** Type C shale, Well D, 2447.33 m; **(I)** Type C shale, Well E,1750.73 m.

Inorganic pore

According to the observation of argon ion polishing scanning electron microscopy, there are four types of inorganic pores developed in the lacustrine shale of Lianggaoshan Formation in the study area, including interparticle pore between grains, intraplatelet pore within clay aggregates, intercrystalline pore within pyrite framboids and intraparticle pore (Figure 3).

The interparticle pore is one of the main pore types of lacustrine shale in the Lianggaoshan Formation (Figure 3A). It is a primary pore between quartz, feldspar, clay minerals (such as illite, chlorite, etc.) and other particles arranged and accumulated, and remained after diagenetic compaction (Figure 3B). Through observation and analysis, it is shown that the micro-pores developed between mineral particles and between mineral particles and clay minerals in the study area are mainly triangular, polygonal, elongated and irregular in shape. The pore size range is large, nano-scale and micron-scale pores are developed, mainly formed by the contact of brittle particles and plastic particles. Since most of the intergranular pores with large pore size in the early stage were filled with asphalt, only part of the intergranular pores with relatively small pore size remained, which were preserved by a certain compressive supporting structure formed by the disorderly accumulation of clay minerals and brittle particles or clay minerals.

Intraplatelet pore is the micropore within illite and chlorite (Figure 3A). When shale pore water is alkaline and rich in potassium ions, montmorillonite will convert to illite as the burial depth increases, accompanied by a decrease in volume, resulting in intraplatelet pore. Intraplatelet pores are widely developed in lacustrine shale of Lianggaoshan Formation (Figure 3C), which are generally developed between illite lamellae and between illite and mica lamellae (Figure 3D). This type of pore morphology can be slit, triangle or polygon (Figure 3E). The formation of this kind of pores is caused by the early clay mineral pores (Figure 3F). With the increase of burial depth, the intraplatelet pore decreases rapidly under strong compaction.

Intraparticle pore is a secondary pore generated by the dissolution of soluble minerals such as feldspar and carbonate by acidic fluid produced after decarboxylation of organic matter (Figure 3B). The intraparticle pore size is relatively small, mainly between 0.05um and 4um (Figure 3G).

Intercrystalline pore within pyrite framboids is an intergranular micropore formed by mineral crystallization under stable environment and suitable medium conditions (Figures 3H, I). In general, the inorganic pores in Type A shale are mainly intraparticle pore, intercrystalline pore within pyrite framboids and interparticle pore, and the pore size of inorganic pores is more than 1 μm. The inorganic pores of Type C shale are mainly intraparticle pore, interparticle pore and intercrystalline pore within pyrite framboids. In contrast, Type B shale has the lowest development of inorganic pores.

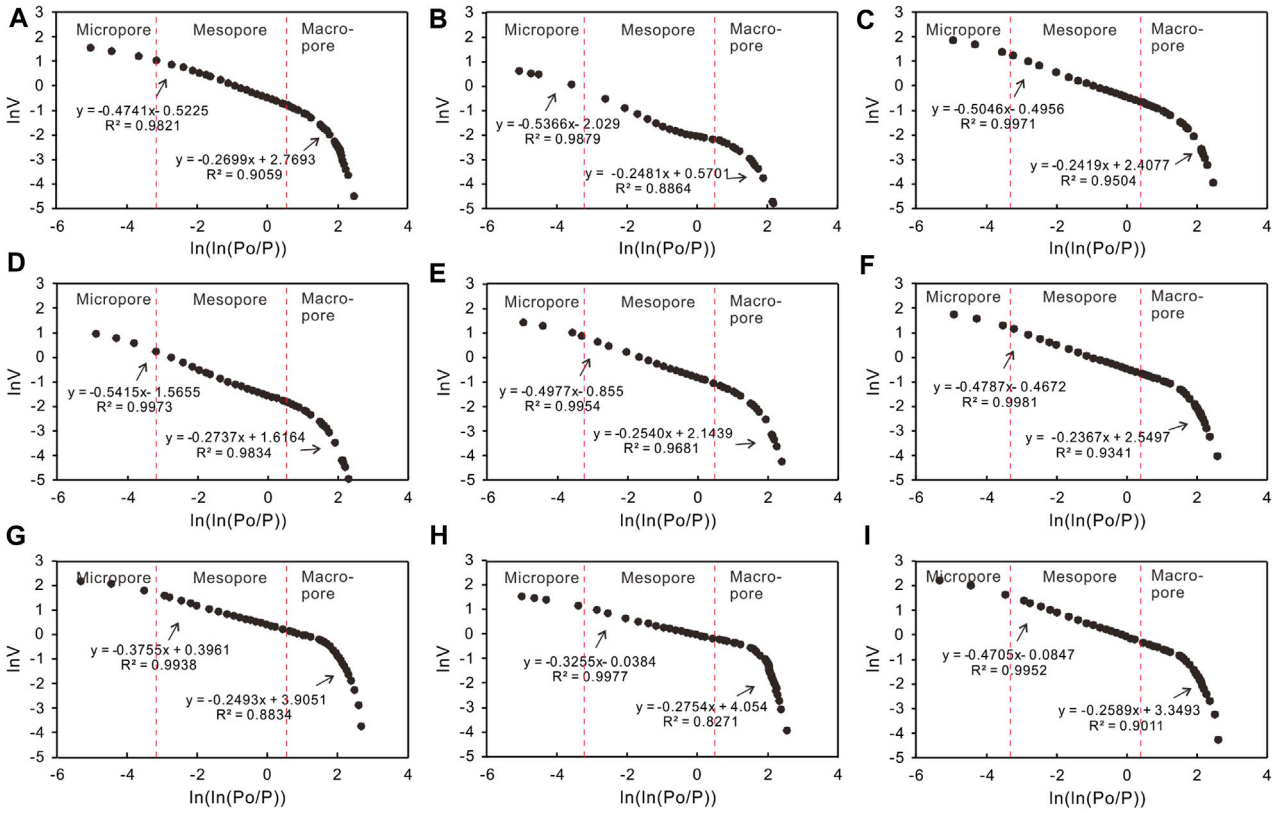

FIGURE 9
Schematic diagram showing fractal fitting of Jurassic Lianggaoshan Formation lacustrine shale in different lithology combination. Micropore, mesopore, and macropore are represented as the blue, red, and black hollow circles, respectively. **(A)** Type A shale, Well A, 2161.25 m; **(B)** Type A shale, Well B, 2455.06 m; **(C)** Type A shale, Well C, 1764.7 m; **(D)** Type B shale, Well D, 2437.33 m; **(E)** Type B shale, Well E, 1751.71 m; **(F)** Type B shale, Well C, 1894.02 m; **(G)** Type C shale, Well A, 2164.49 m; **(H)** Type C shale, Well D, 2465.48 m; **(I)** Type C shale, Well C, 1928.58 m

Microfracture

The microfractures developed in shale reservoirs are not only conducive to the enrichment of free gas, but also the main channel for shale gas seepage and migration, which plays a key role in the development of shale gas. According to the genesis of fractures, the microfractures in lacustrine shale of Lianggaoshan Formation can be divided into bedding fracture, shrinkage fracture and structural fracture (Figure 4).

Proportion of different reservoir spaces

Organic pores are generally lipophilic, while inorganic pores are mostly hydrophilic (Li et al., 2016). Tinni et al. (2014) used nuclear magnetic resonance experiments to identify the distribution characteristics of transverse relaxation time (T_2) of oil-wet pores and hydrophilic pores in shale gas reservoirs. It is generally believed that organic pores in shale gas reservoirs have strong oil wettability, while inorganic pores have strong water wettability. Accordingly, NMR experiments were conducted under water- and oil-saturated conditions, respectively, to observe the signal characteristics on the transverse relaxation time (T_2) distribution spectra of the two types of pores. The presence of three peaks in the T_2 spectra of lipophilic pores indicates three types of organic pores: volumetrically dominant small pores with short T_2, large pores with long T_2, and microfracture developed in organic matter (Figure 5). Based on the above theoretical understanding, Fu et al. (2021) proposed a method for calculating the proportion of organic and inorganic pores based on the wettability of shale pores.

The T_2 spectrum shows that the Type A shale saturated by oil exhibits unimodal characteristics, and the corresponding amplitude is high. The calculation results suggest that the organic pores account for 26.02% of all reservoir spaces, and the inorganic pores account for 34.46%. The T_2 spectrum shows that the Type B shale saturated by oil is also unimodal shape, the corresponding amplitude is low, and the organic pores only account for 1.82%. The T_2 spectrum shows that the Type C shale saturated by oil is unimodal shape. The corresponding amplitude is relatively higher than Type B shale. When shale sample is saturated with water, the corresponding amplitude exhibits much higher than shale sample saturated with oil. The organic pores in Type C shale account for 19.00% (Figure 6).

Pore structure quantitative characteristics

LTNA isotherms

The IUPAC classification of LTNA curves and hysteresis loops divides nanoscale pores into four different categories, i.e., cylindrical pores, ink bottle pores, parallel plate pores, and slit pores (Thommes et al., 2015). Results suggest that Type C shale

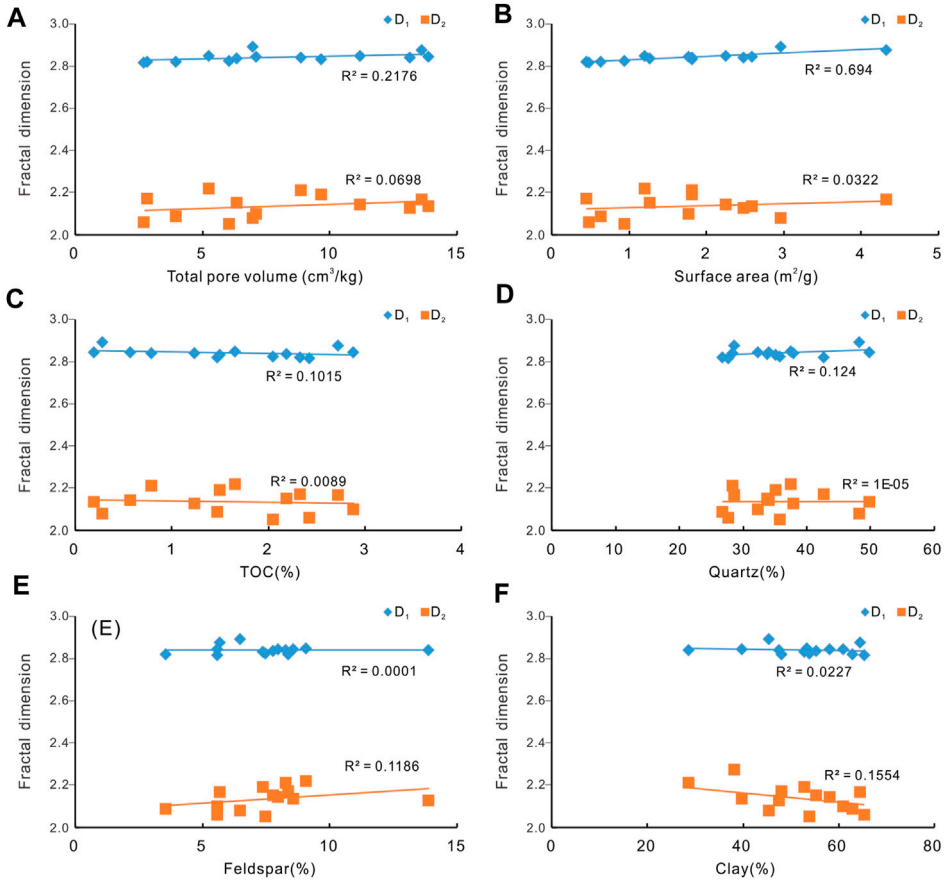

FIGURE 10
Correlation between the shale mineral composition and fractal dimension of the Jurassic Lianggaoshan Formation lacustrine shale. **(A)** Correlation between fractal dimensions and total pore volumn; **(B)** Correlation between fractal dimensions and surface area; **(C)** Correlation between fractal dimensions and TOC content; **(D)** Correlation between fractal dimensions and quartz content; **(E)** Correlation between fractal dimensions and feldspar content; **(F)** Correlation between fractal dimensions and clay content.

is dominated by parallel plate pores with high development and good connectivity. The Type A shale is dominated by parallel plate pores with lower development than Type C. The Type B shale is dominated by parallel plate pores with lowest development. Figures 7, 8.

Surface area (SA) and pore volume (PV)

The surface area of the Lianggaoshan shale samples were acquired through the BET model. The surface area of the Type C shale ranges from 0.48 m^2/g to 4.32 m^2/g and the SA of the Type B ranges from 0.63 m^2/g to 1.82 m^2/g. The surface area of the Type A shale ranges from 0.44 m^2/g to 1.81 m^2/g.

The pore volume range of the Lianggaoshan shale is between 2.73 cm^3/kg and 13.90 cm^3/kg (average value 7.99 cm^3/kg). The average pore volume of the Type A and Type B is 6.23 cm^3/kg and 6.33 cm^3/kg, lower than that of the Type C shale (10.28 cm^3/kg).

Pore-size distribution (PSD)

The PSD between 2nm and 100000 nm was acquired by integrating MICP and LTNA experiments. The results show that although the reservoir space of Lianggaoshan lacustrine shale is mainly mesopores ranging between 10nm and 50 nm and macropores ranging between 50nm and 100 nm.

Discussion

Through correlationship between shale reservoir key parameters and fractal dimension, the main controlling factors of pore structure are discussed. The fractal dimension D_1 reflects relative pressure (P/P_o) > 0.5, representing capillary condensation. The fractal dimension D_2 reflects relative pressure (P/P_o) < 0.5, representing mono- and multi-layer adsorption (Figure 9).

For Lianggaoshan shale, the D_1 reflects the micropore development, and D_2 reflects the development degree of mesopore-macropore. D_2 is generally larger than D_1 and is closer to 3, suggesting that the mesopore-macropore has a simpler pore structure than micropore, and its heterogeneity is weaker. D_1 is characterized by clearly positive correlation with SA and PV, suggesting micropores are major contributors to SA and PV of Lianggaoshan shale (Figures 10A, B).

The correlation between TOC and D_1 is slightly positive, indicating that the enrichment of organic matter has little effect on the formation of micropores (Figure 10C). In addition, the enrichment of organic matter does not affect the mesopore-macropore development as well. Due to the low content of quartz in Lianggaoshan lacustrine shale, which is mainly detrital quartz, it does not significantly affect the formation of micropore and mesopore-macropore (Figure 10D). A slight positive correlation exists between D_2 and feldspar content, indicating that intraparticle pores developed in feldspar particles provide partial mesopore-macropore but not micropores (Figure 10E). There is no correlationship between clay mineral content and D_1, suggesting clay minerals has no perceptible effect on the formation of micropore. Meanwhile, there is a slightly negative correlationship between clay mineral and D_2, suggesting the existence of clay minerals is unfavorable to the development of mesopore-macropore (Figure 10F).

Conclusions

1) Three types of lithology combination developed in the Jurassic Liangggaoshan lacustrine shale. Type A comprises pure shale. Type B is characterized by frequent shell limestone interbedding. Type C is characterized by frequent siltstone interbedding.

2) Organic pore, inorganic pore (including intraparticle pore in feldspar, interparticle pore, and intercrystalline pore between pyrite crystals), and microfractures compose reservoir spaces of Jurassic Liangggaoshan lacustrine shale. Type A shale has the highest proportion of organic pores, while Type B has the lowest proportion. The pores of Lianggaoshan lacustrine shales are dominated by mesopores and part of the macropores. Among them, the PV and SA are both mainly dominated by micropores.

3) The enrichment of organic matter has little effect on the development of micropores, and does not affect the mesopore and macropore development as well. Quartz particles in Lianggaoshan lacustrine shale do not clearly facilitate the development of micropore and mesopore-macropore. Intraparticle pore in feldspar clast is an important component of mesopore and macropore. Clay minerals has no positive effect on the formation of micropore and mesopore-macropore.

Data availability statement

The raw data supporting the conclusion of this article will be made available by the authors, without undue reservation.

Author contributions

QL contributed as the major author of the article. SM, YZ, and PF conceived the project. SL, JH, and JZ collected the samples. RY and SC analyzed the samples. All authors contributed to the article and approved the submitted version.

Funding

The study was funded by the National Science Foundation of China (Grant Nos. 41302101 and 41330313), the Chuanqing Drilling Engineering Co., Ltd. E Class Scientific Research Project (Grant No. CQ2022B-Y-1-1) and the 973 Prophase Special Program of China (Grant No. 2011CB211701) is acknowledged. The authors declare that this study received funding from the Chuanqing Drilling Engineering Co., Ltd. The funder was not involved in the study design, collection, analysis, interpretation of data, the writing of this article or the decision to submit it for publication.

Conflict of interest

Authors QL, LQ, SC, and RY were employed by the CNPC Chuanqing Drilling Engineering Co., Ltd; Authors SM, YZ, and PF were employed by the PetroChina Southwest Oil and Gas Field Company; Author SL was employed by the Sichuan Yuesheng Energy Group Co., Ltd; Author JH was employed by the Chengdu Geoservice Oil and Gas Technology Development Company; Author JZ was employed by the Chengdu Caledonian Oil and Gas Technology Development Co., Ltd.

Publisher's note

References

Cai, G., Jiang, Y., Li, X., Sun, S., Fu, Y., Gu, Y., et al. (2022). Comparison of characteristics of transitional and marine organic-rich shale reservoirs. *Acta Sedimentol. Sin.* 40 (4), 1030–1042. doi:10.14027/j.issn.1000-0550.2021.069

Chen, D., Zhang, J., Wang, X., Lan, B., Li, Z., and Liu, T. (2018). Characteristics of lacustrine shale reservoir and its effect on methane adsorption capacity in Fuxin Basin. *Energy and Fuels* 32 (11), 11105–11117. doi:10.1021/acs.energyfuels.8b01683

Cheng, D., Zhang, Z., Hong, H., Zhang, S., Qin, C., Yuan, X., et al. (2023). Sedimentary and provenance characteristics and the basin-mountain relationship of the jurassic Lianggaoshan Formation in eastern Sichuan Basin, SW China. *Petroleum Explor. Dev.* 50 (2), 1–11. doi:10.11698/PED.20220412

Dong, D., Liang, F., Guan, Q., Jiang, Y., Zhou, S., Yu, R., et al. (2022). Development model and identification evaluation technology of Wufeng-Longmaxi Formation quality shale gas reservoirs in the Sichuan Basin. *Nat. Gas. Ind.* 42 (8), 96–111. doi:10.3787/j.issn.1000-0976.2022.08.008

Fan, C., Li, H., Qin, Q., He, S., and Zhong, C. (2020). Geological conditions and exploration potential of shale gas reservoir in Wufeng and Longmaxi Formation of southeastern Sichuan Basin, China. *J. Petroleum Sci. Eng.* 191, 107138. doi:10.1016/j.petrol.2020.107138

Fan, C., Xie, H., Li, H., Zhao, S., Shi, X., Liu, J., et al. (2022). Complicated fault characterization and its influence on shale gas preservation in the southern margin of the Sichuan Basin, China. *Lithosphere* 2022, 8035106. doi:10.2113/2022/8035106

Fu, Y., Jiang, Y., Dong, D., Hu, Q., Lei, Z., Peng, H., et al. (2021). Microscopic pore-fracture configuration and gas-filled mechanism of shale reservoirs in the Western chongqing area, Sichuan Basin, China. *Petroleum Explor. Dev.* 48 (5), 1063–1076. doi:10.1016/S1876-3804(21)60091-5

Fu, Y., Jiang, Y., Xia, G., Chen, H., Zhou, K., Wang, J., et al. (2020). Optimization of GRI porosity determination method for marine shale. *Nat. Gas. Ind.* 40 (10), 20–28. doi:10.3787/j.issn.1000-0976.2020.10.003

Gu, Y., Cai, G., Hu, D., Wei, Z., Liu, R., Han, J., et al. (2022c). Geochemical and geological characterization of upper permian linghao Formation shale in nanpanjiang basin, SW China. *Front. Earth Sci.* 10, 883146. doi:10.3389/feart.2022.883146

Gu, Y., Hu, D., Wei, Z., Liu, R., Hao, J., Han, J., et al. (2022b). Sedimentology and geochemistry of the upper permian linghao formation marine shale, central nanpanjiang basin, SW China. *Front. Earth Sci.* 10, 914426. doi:10.3389/feart.2022.914426

Gu, Y., Li, X., Qi, L., Li, S., Jiang, Y., Fu, Y., et al. (2022a). Sedimentology and geochemistry of the lower permian shanxi formation Shan 2^3 submember transitional shale, eastern Ordos Basin, north China. *Front. Earth Sci.* 10, 859845. doi:10.3389/feart.2022.859845

Guo, X., Borjigin, T., Wei, X., Yu, L., Lu, X., Sun, L., et al. (2022b). Occurrence mechanism and exploration potential of deep marine shale gas in Sichuan Basin. *Acta Pet. Sin.* 43 (4), 453–468. doi:10.7623/syxb202204001

Guo, X., Hu, D., Shu, Z., Li, Y., Zheng, A., Wei, X., et al. (2022a). Exploration, development and construction in the Fuling national shale gas demonstration area in Chongqing: Progress and prospect. *Nat. Gas. Ind.* 42 (8), 14–23. doi:10.3787/j.issn.1000-0976.2022.08.002

Han, H., Dai, J., Guo, C., Zhong, N., Pang, P., Ding, Z., et al. (2021). Pore characteristics and factors controlling lacustrine shales from the upper cretaceous Qingshankou formation of the Songliao Basin, northeast China: A study combining SEM, low-temperature gas adsorption and MICP experiments. *Acta Geol. Sin. Engl. Ed.* 95 (2), 585–601. doi:10.1111/1755-6724.14419

Huang, H., Li, R., Lyu, Z., Cheng, Y., Zhang, B., Jiang, Z., et al. (2022). Comparative study of methane adsorption of Middle-Upper Ordovician marine shales in the Western Ordos Basin, NW China: Insights into impacts of moisture on thermodynamics and kinetics of adsorption. *Chem. Eng. J.* 446, 137411. doi:10.1016/j.cej.2022.137411

Jiang, Y., Chen, L., Qi, L., Luo, M., Chen, X., Tao, Y., et al. (2018). Characterization of the lower silurian longmaxi marine shale in changning area in the south Sichuan Basin, China. *Geol. J.* 53, 1656–1664. doi:10.1002/gj.2983

Jiang, Y., Song, Y., Qi, L., Chen, L., Tao, Y., Gan, H., et al. (2016). Fine lithofacies of China's marine shale and its logging prediction: A case study of the lower silurian longmaxi marine shale in weiyuan area, southern Sichuan Basin, China. *Earth Sci. Front.* 23 (1), 107–118. doi:10.13745/j.esf.2016.01.010

Lei, W., Chen, D., Liu, Z., and Cheng, M. (2023). Paleoenvironment-driven organic matter accumulation in lacustrine shale mixed with shell bioclasts: A case study from the jurassic da'anzhai member, Sichuan Basin (China). *J. Petroleum Sci. Eng.* 220, 111178. doi:10.1016/j.petrol.2022.111178

Li, H. (2022). Research progress on evaluation methods and factors influencing shale brittleness: A review. *Energy Rep.* 8, 4344–4358. doi:10.1016/j.egyr.2022.03.120

Li, H., Zhou, J., Mou, X., Guo, H., Wang, X., An, H., et al. (2022a). Pore structure and fractal characteristics of the marine shale of the longmaxi Formation in the changning area, southern Sichuan Basin, China. *Front. Earth Sci.* 10, 1018274. doi:10.3389/feart.2022.1018274

Li, J., Jin, W., Wang, L., Wu, Q., Lu, J., and Hao, S. (2016). Quantitative evaluation of organic and inorganic pore size distribution by NMR: A case from the silurian longmaxi formation gas shale in fuling area,Sichuan Basin. *Oil Gas Geol.* 37 (1), 129–134. doi:10.11743/ogg20160118

Li, J., Li, H., Yang, C., Wu, Y., Gao, Z., and Jiang, S. (2022b). Geological characteristics and controlling factors of deep shale gas enrichment of the Wufeng-Longmaxi Formation in the southern Sichuan Basin, China. *Lithosphere* 2022 (12), 4737801. doi:10.2113/2022/4737801

Li, Y., Zhou, A., Xie, W., Qiu, X., Dai, Y., Hu, X., et al. (2022c). Lithofacies divisionand main controlling factors of reservoir development in Wufeng Formation-Longilsub-member shale in the Luzhou region, South Sichuan Basin. *Nat. Gas. Ind.* 42 (8), 112–123. doi:10.3787/j.issn.1000-0976.2022.08.009

Liu, Y., Huang, C., Zhou, Y., Lu, Y., and Ma, Q. (2020). The controlling factors of lacustrine shale lithofacies in the Upper Yangtze Platform (South China) using artificial neural networks. *Mar. Pet. Geol.* 118, 104350. doi:10.1016/j.marpetgeo.2020.104350

Liu, Z., Hu, Z., Liu, G., Liu, Z., Liu, H., Hao, J., et al. (2021). Pore characteristics and controlling factors of continental shale reservoirs in the Lower Jurassic Ziliujing Formation, northeastern Sichuan Basin. *Oil Gas Geol.* 42 (1), 136–145. doi:10.11743/ogg20210112

Loucks, R. G., Reed, R. M., Ruppel, S. C., and Hammes, U. (2012). Spectrum of pore types and networks in mudrocks and a descriptive classification for matrix-related mudrock pores. *AAPG Bulltin* 96 (6), 1071–1098. doi:10.1306/08171111061

Peng, J., Hu, Z., Feng, D., and Wang, Q. (2022). Sedimentology and sequence stratigraphy of lacustrine deep-water fine-grained sedimentary rocks: The lower jurassic Dongyuemiao Formation in the Sichuan Basin, western China. *Mar. Petroleum Geol.* 146, 105933. doi:10.1016/j.marpetgeo.2022.105933

Qiu, Z., and He, J. (2022). Depositional environment changes and organic matter accumulation of Pliensbachian-Toarcian lacustrine shales in the Sichuan basin, SW China. *J. Asian Earth Sci.* 232, 105035. doi:10.1016/j.jseaes.2021.105035

Rouquerol, J., Avnir, D., Fairbridge, C. W., Everett, D. H., Haynes, J. H., Pernicone, N., et al. (1994). Recommendations for the characterization of porous solids (Technical Report). *Pure Appl. Chem.* 66, 1739–1758. doi:10.1351/pac199466081739

Shu, Z., Zhou, L., Li, X., Liu, H., Zeng, Y., Xie, H., et al. (2021). Geological characteristics of gas condensate reservoirs and their exploration and development prospect in the Jurassic continental shale of the Dongyuemiao Member of Ziliujing Formation, Fuxing area, eastern Sichuan Basin. *Oil Gas Geol.* 42 (1), 212–223. doi:10.11743/ogg20210118

Sun, W., Feng, Y., Jiang, C., and Chu, W. (2015). Fractal characterization and methane adsorption features of coal particles taken from shallow and deep coalmine layers. *Fuel* 155, 7–13. doi:10.1016/j.fuel.2015.03.083

Sun, Y., Jiang, Y., Xiong, X., Li, X., Li, S., Qiu, Z., et al. (2022). Lithofacies and sedimentary environment evolution of the Shan23 Submember transitional shale of the Shanxi Formation in the Danilng-Jixian area, eastern Ordos Basin. *Coal Geol. Explor.* 50 (9), 104–114. doi:10.12363/issn.1001-1986.21.12.0821

Thommes, M., Kaneko, K., Neimark, A. V., Olivier, J. P., Rodriguez-Reinoso, F., Rouquerol, J., et al. (2015). Physisorption of gases, with special reference to the evaluation of surface area and pore size distribution (IUPAC Technical Report). *Pure Appl. Chem.* 87, 1051–1069. doi:10.1515/pac-2014-1117

Tinni, A., Odusina, E., and Sulucamain, I. (2014). "NMR response of brine, oil, and methane in organic rich shales," in *SPE USA unconventional resources conference: The woodlands* (Texas, USA: SPE), 98–106.

Wang, M., Xue, H., Tian, S., Wilkins, R. W. T., and Wang, Z. (2015). Fractal characteristics of upper cretaceous lacustrine shale from the Songliao Basin, NE China. *Mar. Petroleum Geol.* 67, 144–153. doi:10.1016/j.marpetgeo.2015.05.011

Wang, X., Jin, Z., Zhao, J., Zhu, Y., Hu, Z., Liu, G., et al. (2020). Depositional environment and organic matter accumulation of Lower Jurassic nonmarine fine-grained deposits in the Yuanba Area, Sichuan Basin. SW China. *Mar. Petroleum Geol.* 116, 104352. doi:10.1016/j.marpetgeo.2020.104352

Wang, Z., Jiang, Y., Fu, Y., Lei, Z., Xu, C., Yuan, J., et al. (2022). Characterization of pore structure andheterogeneity of shale reservoir from Wufeng Formation-Sublayers Long-1, in Western Chongqing based on nuclear magnetic resonance. *Earth Sci.* 47 (2), 490–504. doi:10.3799/dqkx.2021.076

Wei, G., Wang, W., Feng, L., Tan, X., Yu, C., Zhang, H., et al. (2021). Geological characteristics and exploration prospect of black shale in the Dongyuemiao member of lower jurassic, the eastern Sichuan Basin, China. *Front. Earth Sci.* 9, 765568. doi:10.3389/feart.2021.765568

Xi, Z., Tang, S., Wang, J., Yang, G., and Li, L. (2018). Formation and development of pore structure in marine-continental transitional shale from northern China across a maturation gradient: Insights from gas adsorption and mercury intrusion. *Int. J. Coal Geol.* 200, 87–102. doi:10.1016/j.coal.2018.10.005

Xi, Z., Tang, S., Zhang, S., Lash, G. G., and Ye, Y. (2022). Controls of marine shale gas accumulation in the eastern periphery of the Sichuan Basin, South China. *Int. J. Coal Geol.* 251, 103939. doi:10.1016/j.coal.2022.103939

Xu, Q., Liu, B., Ma, Y., Song, X., Wang, Y., and Chen, Z. (2017). Geological and geochemical characterization of lacustrine shale: A case study of the jurassic Da'anzhai member shale in the central Sichuan Basin, Southwest China. *J. Nat. Gas Sci. Eng.* 47, 124–139. doi:10.1016/j.jngse.2017.09.008

Yang, R., Hu, Q., Yi, J., Zhang, B., He, S., Guo, X., et al. (2019). The effects of mineral composition, TOC content and pore structure on spontaneous imbibition in Lower Jurassic Dongyuemiao shale reservoirs. *Mar. Petroleum Geol.* 109, 268–278. doi:10.1016/j.marpetgeo.2019.06.003

Yuan, T., Wei, X., Zhang, H., Li, C., Wei, F., Lu, L., et al. (2022). Shale petrofacies division of Wufeng-Longmaxi formations in Sichuan Basin and its periphery. *Petroleum Geol. Exp.* 42 (3), 371–414. doi:10.11781/sysydz202003371

Zhang, P., Lu, S., Li, J., Wang, J., Zhang, J., Chen, G., et al. (2023). Microscopic characteristics of pore-fracture system in lacustrine shale from Dongying Sag, Bohai Bay Basin, China: Evidence from scanning electron microscopy. *Mar. Petroleum Geol.* 150, 106156. doi:10.1016/j.marpetgeo.2023.106156

Zhang, P., Lu, S., Li, J., Chang, X., Li, J., Li, W., et al. (2020). Broad ion beam-scanning electron microscopy pore microstructure and multifractal characterization of shale oil reservoir: A case sample from dongying sag, Bohai Bay Basin, China. *Energy Explor. Exploit.* 38, 613–628. doi:10.1177/0144598719893126

Zhang, P., Misch, D., Hu, F., Kostoglou, N., Sachsenhofer, R. F., Liu, Z., et al. (2021). Porosity evolution in organic matter-rich shales (Qingshankou Fm.; Songliao Basin, NE China): Implications for shale oil retention. *Mar. Petroleum Geol.* 130, 105139. doi:10.1016/j.marpetgeo.2021.105139

Zhao, X., Zhou, L., Pu, X., Jin, F., Han, W., Shi, Z., et al. (2022). Theories, technologies and practices of lacustrine shale oil exploration and development: A case study of Paleogene Kongdian Formation in cangdong sag, Bohai Bay Basin, China. *Petroleum Explor. Dev.* 49 (3), 707–718. doi:10.1016/s1876-3804(22)60059-4

Zou, C., Zhu, R., Chen, Z., Ogg, J. G., Wu, S., Dong, D., et al. (2019). Organic-matter-rich shales of China. *Earth Sci. Rev.* 189, 51–78. doi:10.1016/j.earscirev.2018.12.002